IOP Conf. Series: Journal of Physics: Conf. Series **1037** (2018) 052016 doi:10.1088/1742-6596/1037/5/052016

Design of a multipurpose scaled wind turbine model

E M Nanos[1], N Kheirallah[1], F Campagnolo[1] and C L Bottasso[1,2]

[1]Wind Energy Institute, Technische Universität München, Garching bei München, Germany
[2] Dipartimento di Scienze e Tecnologie Aerospaziali, Politecnico di Milano, Milano, Italy

E-mail: em.nanos@tum.de

Abstract. This paper describes the methodology that was followed for designing a scaled wind turbine model. This model is intended to be used in complex terrain studies as well as deep array wind farm control tests. Therefore, emphasis was given on making it as compact as possible while keeping a high level of instrumentation. The result is a three blade wind turbine with rotor diameter of 0.6 m equipped with active pitch, yaw and torque control. After a discussion on the design procedure, we present preliminary performance characteristics of the model obtained experimentally.

1. Introduction

Wind tunnel testing is an invaluable tool for improving wind turbine efficiency and eventually reducing the levelized cost of energy from wind. The wind turbine component that has benefited the most from wind tunnel testing is certainly the blade, since wind tunnel testing of wind turbine airfoils was used from the very beginning of the wind energy industry [1]. However, wind tunnel testing embraced over the years more aspects of wind turbine design, going one step further from airfoil performance experiments to testing of scaled wind turbine models. Indeed, wind tunnel testing of scaled wind turbines has been used for a plethora of applications such as wake studies [2, 3], wind turbine control tests [4], wind farm control validation [5] and complex terrain studies [6]. Undoubtedly, scaled wind turbine model design evolved over the years following the demand for new research applications. For example, in the MEXICO project [2, 3] a 4.5 m diameter wind turbine model was developed with highly instrumented blades with the purpose of creating a database of wake and rotor load data. In other wake studies smaller scaled wind turbines were used, such as the 10 cm diameter model that Chamoro et al. used in [7] or the 15 cm model developed by Bastankhah in [8]. Models of similar size have been used for simulating wind farms in a wind tunnel, as for example the nine scaled models of 12 cm rotor diameter used for simulating a 3×3 array in [9]. In [4], an aeroelastically scaled model of a Vestas V90 wind turbine was developed, featuring a 2 m rotor diameter and active torque, yaw and individual pitch control. In [5], a model with similar control capabilities but a smaller rigid rotor (1.1 m diameter) and flexible tower was developed.

The above list, although not exhaustive, reveals the great diversity of scaled wind turbine models that exist in the literature. Some of them are quite sophisticated in terms of design and instrumentation, yet their size requires large wind tunnels and/or limits the number of wind turbines that can be used to avoid blockage or other undesirable effects. Some others are quite small and, despite being very useful for wind farm aerodynamic studies, they have limited capabilities and/or aerodynamic performance. In this paper we introduce a multipurpose scaled

wind turbine model whose goal is to bring together compact size and sufficient instrumentation, including active pitch, torque and yaw control and load sensors in multiple parts of the model, while ensuring a realistic process of generating torque from wind. The size and the capabilities of the model make it suitable for a variety of studies that include, but are not limited to, complex terrain, turbine interactions, wind farm control tests, wake studies etc. The paper is organized as follows: first in section 2 the design methodology is described, then section 3 presents the main characteristics of the model, followed by section 4 that gives a preliminary discussion of the model performance; finally, section 5 gives an outlook of the next steps of this activity.

2. Design methodology

The rotor is evidently the most important part of the model and the one that drives its applicability. Consequently, the intended use of the model, as described above, dictates a number of requirements:

- The rotor diameter should allow for the use of the models in complex terrain studies and deep array wind farm tests in which wind farm control algorithms will be studied. Previous studies [10, 11] have shown that in aligned conditions (a column of wind turbines aligned with the main wind direction) the wind turbine power output decreases rapidly and then converges to a fairly constant value after the 5th to 7th wind turbine (depending on the spacing between them). Therefore, taking into account the space restrictions of the atmospheric boundary layer wind tunnel at Politecnico di Milano, we set a requirement of 6 aligned turbines with a spacing of 4 diameters.
- A similar wake behavior to a full scale reference model is desired. Wake similarity translates into kinematic and dynamic similarity of the flow past the wind turbine rotor. Kinematic similarity means that the streamlines of the flow are geometrically similar for full scale and model wind turbine and this can be achieved by keeping the tip speed ratio the same. Dynamic similarity is far more complex and for rotor aerodynamics it requires geometric similarity of the blade geometry and equality of the flow Reynolds number. Given that the geometric scaling factor of the model is around $1 : \mathcal{O}(200)$ (compared to typical modern full scale machines), matching the Reynolds number would require wind speed or density (pressure) that are far beyond the capabilities of atmospheric boundary layer wind tunnels. It is clear that a different approach should be followed. Vortex theory (that has been used extensively for predicting loads on helicopter rotors) suggests that the bound circulation on the blade segments dictates the wake evolution. Besides, as demonstrated in [7], the flow first order statistics in the far wake (which is a region of interest for wind farm operation) become independent of the Reynolds number for Re above $Re_D \approx 10^5$ ($Re_D = DU_{hub}/\nu$ where D is the rotor diameter, U_{hub} is the incoming wind speed at hub height and ν is the kinematic viscosity of air), which is much lower than the expected Re_D of the model throughout its operational regime. In the light of the above, we decided to disregard any geometric similarity requirement (mainly by choosing more appropriate airfoil as described later on), relax the Reynolds number equality requirement and match the non-dimensional circulation distribution along the blade of the reference model, an approach that has been followed by Hassanzadeh et al. in [12] as well. The dimensionless circulation along the span can be defined as:
$$\Gamma' = \frac{C_l}{2}\frac{c}{R}\frac{W}{U}, \tag{1}$$
where C_l is the lift coefficient, c is the chord length , W and U are relative and free stream velocities, respectively. The rotor of the DTU 10-MW wind turbine [13] is used as reference.

Given the requirements and the constraints listed above, we adopted the following procedure:

1. *Airfoil selection.* Inevitably, the model is going to work at low Reynolds, therefore we opted for the RG-14 airfoil, which is a low Reynolds profile with 1.6% maximum camber and 9% maximum thickness at 36% and 31% chord, respectively [15]. In addition, RG-14 is used by another scaled wind turbine model designed at TUM for which we have access to significant performance data sets. This information was used for tuning the airfoil polars, following the procedure proposed by Bottasso et al. in [14]. The obtained airfoil polars were then used for the design and performance validation of the rotor.
2. *Blade sizing.* Chord and twist distributions that maximize the power coefficient C_p are calculated by solving the Blade Element Momentum equations (accounting for tip and root losses). The rated tip speed ratio was set to $\lambda_{\text{rated}} = 8$, equal to the one of the reference model, while the rated rotor speed was set to $\Omega_{\text{rated}} = 2500$ rpm, which was a compromise between hardware limitations and low Reynolds number. The resulting blade geometry is then used as an initial point for the following optimization problem:

$$C^*_{p_i} = \max_{\beta_t, c} \text{Cp}_i\left(\beta_t, c, P\right) \quad (\text{and } \beta^*_t, c^* = \arg\max_{\beta_t, c} \text{Cp}_i), \tag{2a}$$

$$\text{s.t.:} \quad Re_{ci} \geq 70000, \tag{2b}$$

$$\Gamma_i = \Gamma_i^{ref.}, \tag{2c}$$

   where subscript i stands for the i^{th} section (element) of the blade. An in-house developed simulation tool receives as a user-defined input a list of parameters $P = \{D, \Omega_{\text{rated}}, \lambda_{\text{rated}}, B\}$, where D and B are rotor diameter and number of blades respectively, and then it seeks the blade twist β_t and chord c distribution that maximizes the power coefficient C_p of the rotor. The optimization problem is solved subjected to the constraints of circulation Γ and Reynolds number Re_c. This means that, for each blade section, the non-dimensional circulation of the model has to be equal to the respective section of the reference model. In addition, the chord based Reynolds number of the same section, $Re_c = c_i w_i/\nu$ (where c_i is the ith section chord length, and w_i is the incoming relative wind speed of that section) should be larger than 70000. The last constraint was imposed in order to ensure that the algorithm will converge to a solution with the maximum achievable Re_c given all other limitations.
3. *Performance evaluation.* The performance of the rotor geometry obtained from the procedure described above was verified using the aeroelastic code `Fastv8` [16]. This verification step is meant to confirm that the constraints mentioned above are satisfied, but also to verify that the model produces enough torque (which is essential for a precise measurement with the strain gauges) throughout its operational regime. The design and the performance evaluation of the rotor was conducted with the use of tuned airfoil polars.

3. Model characteristics

3.1. General characteristics

The aforementioned design methodology resulted in a wind turbine model (termed G06 for Generic 0.6 m) with the following main dimensions: rotor diameter = 0.6 m, hub diameter = 0.073 m and hub height = 0.61 m. The hub height gives to the G06 a realistic hub height to rotor diameter ratio (around 1.2 for full scale machines), while the dimension of the hub diameter was mainly dictated by the pitch mechanism.

In Fig. 1 (left) the normalized circulation along the blade span is plotted against the target one for a pitch of 0° and $\lambda = 8$. Except for the first 25% of the blade (where it is practically a cylinder) the match is very good. In Fig. 1 (center), the $C_p - \lambda$ curve is plotted for several blade pitch angles at Reynolds 70000. It is worth mentioning that, based on the simulations, the maximum C_p is achieved for $\lambda = 7$ and not 8, which was the initial point of the optimization.

This was somewhat expected, because the tip speed ratio at which the maximum C_p is achieved was not among the optimization constraints.

In Fig. 2 the drivetrain configuration is presented. The rotor blades are connected to the hub, which also houses the pitch mechanism and sensor electronics. The hub is connected to the main shaft, which is fixed to the nacelle with two ball bearings. The slip ring, which is necessary for the transmission of signals from the rotating frame to the stationary frame, is placed in the nacelle together with an optical encoder. The main shaft is connected at its right end with the torque meter, which is then connected with the torque actuator. More details about the sensors can be found in §3.3.

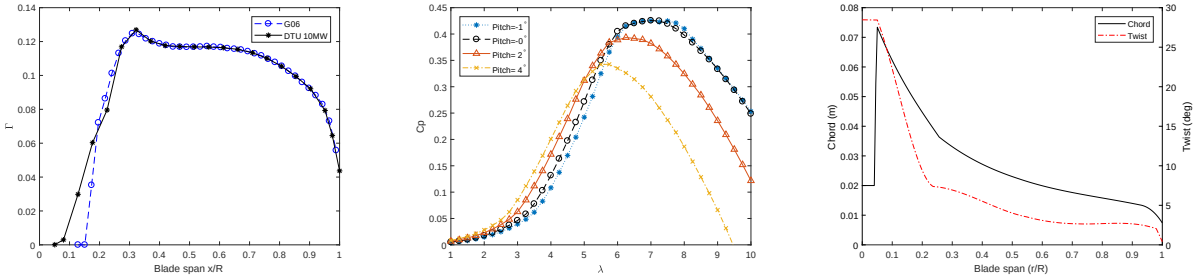

Figure 1: Normalized circulation distribution along the blade for the G06 and DTU 10-MW wind turbines (*left*), C_p vs. tip speed ratio for various pitch angles (*center*) and chord and twist distribution along the blade (*right*).

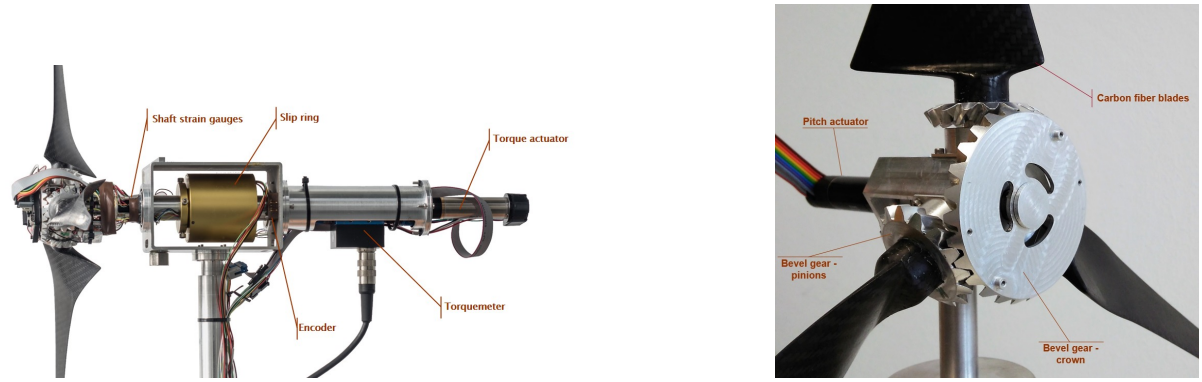

Figure 2: Nacelle (*left*) and hub (*right*). The main components of the hub and the nacelle are marked in the figures.

3.2. Blade manufacturing and pitch mechanism

The blade characteristics (chord and twist distribution) are shown in Fig. 1 (right). The blades (that can be considered rigid) are made from a carbon fiber skin filled with a Rohacell foam core. To this purpose, two aluminium molds where manufactured: one for the pressure and one for the suction side of the blade. The molds where laminated with an appropriate number (depending on the spanwise position) of 0.25 mm thickness carbon fiber plies, while Rohacell foam was used to fill the inside of the blade. Then, the two molds and the bevel gear where fixed and cured together. Since the blades can only be pitched collectively, special attention was

given to the curing process in order to ensure that all blades are identical in terms of relative position with respect to the gear teeth.

The pitching of the blades is performed using a DC motor attached to the hub. The motor is connected to a planetary gear, which is in turn connected through a coupling with the crown of the bevel gear system. The manufacturer of the motor gear provides a value of 1.3° for the motor gear backlash. This means that, when the motor tries to keep the pitch value fixed, the planetary gear allows for a play of 1.3°, which results in a blade pitch play of approximately 2.6°. This could seriously deteriorate the system performance as well as the reliability of the measurements. Therefore, a torsion spring is placed at the root of each blade. This spring is designed to work close to its maximum deflection when the model operates at nominal pitch (0°) and its purpose is to provide a preloading that counteracts the blade pitching moment and keeps the blade fixed to the desired pitch value.

3.3. Sensors

3.3.1. Force and torque sensors The G06 shaft is equipped with three full strain gauge bridges. Two of them are sensitive to shaft bending loads and one of them is sensitive to torsional loading. The bending loads can be used for balancing the rotor and for the detection of shear inflow on the rotor disk [17]. The torsion loads, which are caused by the aerodynamic torque, are used for the evaluation of the rotor performance. Each bridge is connected to a conditioning board mounted on the hub. Signals and power to/from the conditioning boards are transferred to the control unit through a slip ring. In addition to the strain gauges, a high precision commercial torque meter is placed between the main shaft and the generator.

Two additional full bridges are placed at the base of the tower. These bridges are sensitive to the bending loads on the tower. Based on the bending loads one can calculate the rotor thrust using its corresponding arm value. Both shaft and tower bridges are calibrated prior to each experiment by the use of known loads, measuring the voltage output and correlating loads and output with a linear regression.

3.3.2. Position sensors Two kinds of position sensors are used, hall sensors and rotary optical encoders. First, two of the optical encoders are fixed to the torque and pitch actuator, and they are used by the actuator controllers as feedback signals in their closed-loop control scheme. The third optical encoder is placed on the main shaft and it is used for measuring the rotating speed of the model and, most importantly, the azimuthal position of the rotor. Knowledge of the azimuth position is important for interpreting the shaft loads and for performing phase-locked flow measurements.

Second, there is one hall sensor at the root of each blade. The hall sensor is used during the initialization of the system in order to find the zero pitch position (homing). This is necessary because of the torsional springs and the gear backlash, which cause the blades to rest in an unknown position every time the system is switched off. Since the actuator pitch encoder can provide information only on the relative position of the actuator and not the absolute one, the hall sensor is used first to reach a known pitch position, and then the actuator encoder is used to move the blade relative to it. Even though only one hall sensor is necessary, the fact that it is placed in an inaccessible part of the blade makes it necessary to triple the redundancy on this sensor. The relationship between hall sensor output and pitch angle has been established a priori with the following procedure: at first, an inclinometer is fixed on the blade using a metal block designed to fit in a specific blade position, enabling the measurement of the pitch angle. Next, the inclinometer reading and hall sensor output are recorded for several blade pitch angles. Using the recorded values one can establish the desired relationship.

Even though the blades can only be pitched collectively, the procedure described above is repeated for all three blades for two reasons. First, each hall sensor is placed in a slightly

different position, and hence each sensor could have a different output for the same pitch angle. Secondly, the small size of the model, in conjunction with the manufacturing and assembling processes, can cause structural imperfections that can lead to pitch discrepancies among the blades. It is therefore important to verify that all three blades have, with some tolerance, the same pitch angle.

3.3.3. Measurement uncertainty It is crucial for every experimental activity to estimate the error of the obtained results. For the tower and shaft loads, given the sensitivity of the strain gauges and the expected strain within the operational regime, the uncertainty is estimated to be 1%. Similarly, the uncertainty of the torque measurement obtained from strain gauges is estimated to range between 2% and 3%, depending on the operating point. For the torque meter, the manufacturer gives a value of 0.05%, while for the hall sensor the value provided by the manufacturer is below 1%. Regarding the blade pitch angle, given the very small dimensions of the collective pitch mechanism assembly and all the uncertainties that this implies, a tolerance of $\pm 0.3^\circ$ can be estimated. Uncertainties in the dimensions of the model (blade length, tower height etc.) and in the measurement of the rotor angular velocity are considered negligible.

4. Performance measurements

Preliminary wind tunnel measurements were performed in the TUM boundary layer wind tunnel. The test section of this wind tunnel is 1.8 m high, 2.7 m wide and has a length of 21 m. More details about the wind tunnel can be found in the work of Kozmar [18]. The performance was evaluated for average Reynolds numbers $Re_c = 30000$, $Re_c = 40000$ and $Re_c = 50000$. These values, even though lower than the Reynolds at the design point, are expected to be the most common during tests of several models in wind farm configurations or in complex topography installations. Given that chord based Reynolds is not constant along the blade, mainly due to the sheared inflow, the definition of the test matrix was done with a $\pm 5\%$ tolerance for Re_c. For each Reynolds value, the model operated at two different pitch angles, namely -1° and 0°.

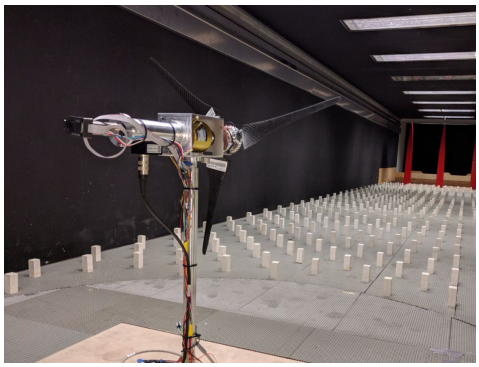

Figure 3: A G06 in the TUM atmospheric boundary layer wind tunnel.

The results of this test in terms of C_p and C_t with respect to λ are presented in Fig. 3, 4 and 5. Results indicate that the C_p curve is very close for the two pitch values, which is expected for λ between 6 and 8. The maximum measured power coefficient is around $C_{p_{\max}} = 0.36$ for Reynolds 30000 and is achieved for tip speed ratio of about 8. For Reynolds 40000 and 50000 the maximum measured C_p is 0.38 and 0.39 for $\lambda = 8$ and 7.5, respectively. The maximum C_p behavior reveals a clear dependency on the Reynolds number, which is also expected based on the fact that airfoil aerodynamic characteristics (and especially drag) are sensitive to Reynolds within this region. The maximum achieved C_p (0.39 for Reynolds 50000) is almost 10% lower than the maximum C_p found during the design phase, at Reynolds 70000 and the same TSR. Part of this difference can be attributed to the difference in the Reynolds number, while manufacturing imperfections on the blade that affect its aerodynamic performance could also play a role. Regarding the thrust coefficient, at tip speed ratio $\lambda = 8$, C_t is equal to 0.85, which is a quite typical value also for a utility scale wind turbine.

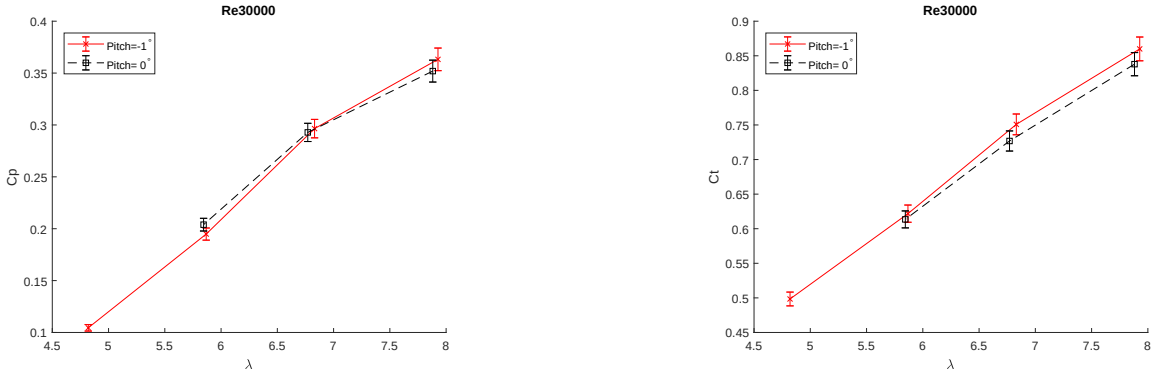

Figure 4: Experimentally obtained C_p vs. λ (*left*) and C_t vs. λ (*right*) for Reynolds 30000.

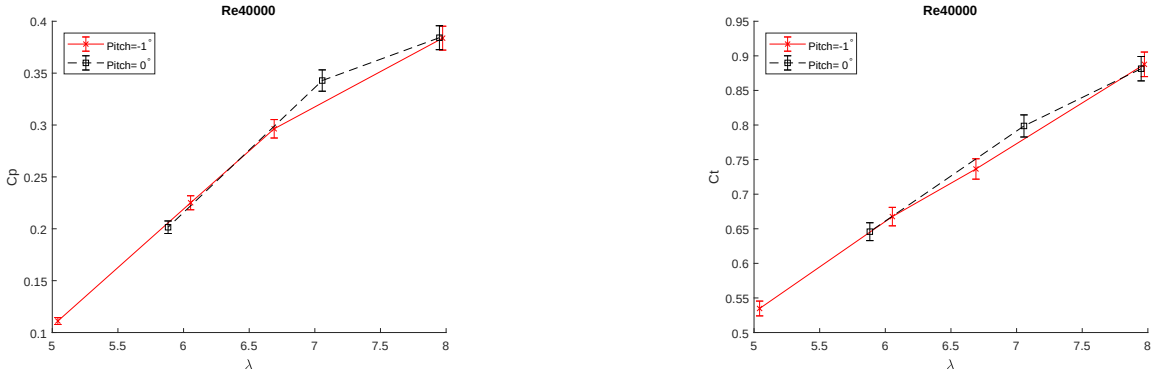

Figure 5: Experimentally obtained C_p vs. λ (*left*) and C_t vs. λ (*right*) for Reynolds 40000.

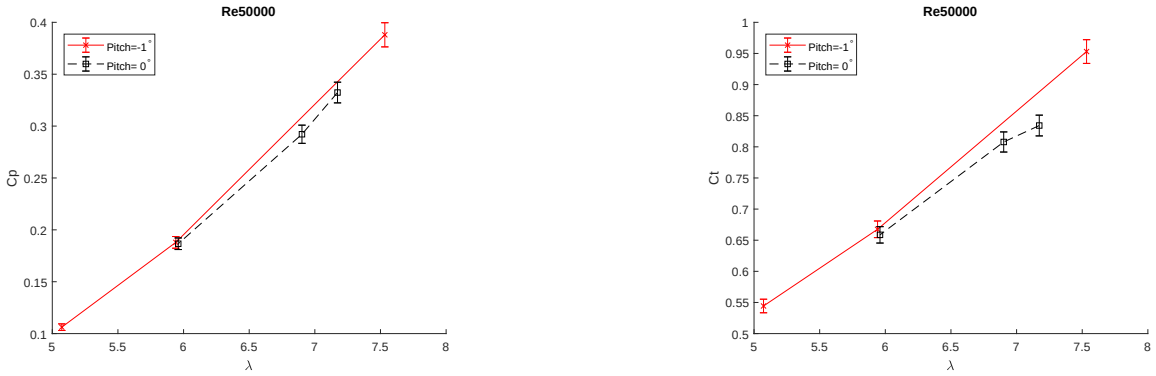

Figure 6: Experimentally obtained C_p vs. λ (*left*) and C_t vs. λ (*right*) for Reynolds 50000.

5. Conclusions

A novel scaled wind turbine model suitable for deep array wind farm configurations and complex terrain tests is presented. The model incorporates a rotor that achieves a wake similarity with the DTU 10 MW reference wind turbine. The model also features torque, pitch and yaw control, which make it suitable for wind turbine and wind farm control experiments. Preliminary

experimental results verified the aerodynamic performance of the rotor and the satisfactory quality of the measurements. However, it is clear that the performance measurements need to be extended with more operating points in order to have more refined and complete C_p-λ and C_t-λ curves, which will allow for more informed conclusions. Future steps in the model characterization process include expansion of the performance curves to the complete operating regime of the model, extensive measurements of the wake, as well as calibration and validation of the wind turbine controller.

6. Acknowledgements

This work has been partially supported by the AWESOME project, which receives funding from the European Union Horizon 2020 research and innovation program under grant agreement No. 642108. The authors would also like to thank Mr. Michael Cerny and Professor Christian Breitsamter for their support during the wind tunnel experiment.

References

[1] Michos A, Bergeles G, Athanassiadis N 1983 Aerodynamic Characteristics of NACA 0012 Airfoil in Relation to Wind Generators *Wind Engineering* **7** 247-262
[2] Snel H, Schepers J and Montgomerie B 2007 The MEXICO Project (Model Experiments in Controlled Conditions): The Database and First Results of Data Processing and Interpretation *J. Phys.: Conf. Series* **75** 012014 IOP Publishing
[3] P Hashemi-Tari et al 2014 Wind Tunnel Investigation of the Near-wake Flow Dynamics of a Horizontal Axis Wind Turbine *J. Phys.: Conf. Series* **524** 012176
[4] Bottasso CL, Campagnolo F, Petrović V. 2014 Wind tunnel testing of scaled wind turbine models: Beyond aerodynamics *J. Wind Eng. Ind. Aerodyn.* **127**, pp. 11–28
[5] Campagnolo F, Petrović V, Schreiber J, Nanos E M, Croce A and Bottasso C L 2016 Wind tunnel testing of a closed-loop wake deflection controller for wind farm power maximization *J. Phys.: Conf. Series* **753** 32006
[6] A Hyvärinen and A Segalini 2017 *J. Phys.: Conf. Series* **854** 012023
[7] Chamorro L P, Arndt R E A and Sotiropoulos F 2011 *Wind Energy* **19** 733–742
[8] Bastankhah M and Porte-Agel F 2017 *Physics of Fluids* **29** 065105
[9] Lebrón J R, Castillo L, Cal R B, Kang H S, Meneveau C 2010 *48th AIAA Aerospace Sciences Meeting*
[10] Stevens R J A M, Gayme D F and Meneveau C 2014 *Journal of Renewable and Sustainable Energy* **06** 023105
[11] Chamorro L P, Arndt R E A and Sotiropoulos F 2011 *Boundary-Layer Meteorology* **141** 349–367
[12] Hassanzadeh A et al 2016 *J. Phys.: Conf. Ser.* **753** 022048
[13] Bak C, Zahle F, Bitsche R, Kim T, Yde A, Henriksen L C, Natarajan A 2013. The DTU 10-MW Reference Wind Turbine [Sound/Visual production (digital)]. Danish Wind Power Research 2013, Fredericia, Denmark, 27/05/2013
[14] Bottasso C L, Cacciola S and Iriarte X 2014. *J. Wind Eng. Ind. Aerodyn.* **124**, pp. 29–45
[15] Lyon A C, Broeren A P, Giguere P, Gopalarathnam A and Selig M 1997. Summary of Low - Speed Airfoil Data *SoarTech Publications*
[16] NWTC Information Portal (FAST v8). https://nwtc.nrel.gov/FAST8
[17] Bottasso C L, Cacciola S and Schreiber J 2018 *Renewable Energy* **116** 155-168.
[18] Kozmar H, *Theor Appl Climatol* 2011 **106** 95-104